Numerical analysis of bent waveguides: bending loss, transmission loss, mode coupling, and polarization coupling

B. M. A. Rahman,[1,*] D. M. H. Leung,[1] S. S. A. Obayya,[2] and K. T. V. Grattan[1]

[1]School of Engineering and Mathematical Sciences, City University London, London EC1V 0HB, UK

[2]School of Electronic and Electrical Engineering, University of Leeds, Leeds LS2 9JT, UK

*Corresponding author: B.M.A.Rahman@city.ac.uk

Received 20 November 2007; revised 24 April 2008; accepted 28 April 2008; posted 28 April 2008 (Doc. ID 90001); published 21 May 2008

A rigorous, full-vectorial and computationally efficient finite-element-based modal solution, together with junction analysis and beam propagation approaches have been used to study bending loss, transition loss, mode coupling, and polarization coupling in bent optical waveguides. The waveguide offset and their widths have been optimized to reduce the transition loss and the mode beating. © 2008 Optical Society of America

OCIS codes: 000.4430, 130.0130, 130.2790, 130.3120, 130.5440.

1. Introduction

In the design of a photonic integrated circuit (PIC), most of the optical components used are assembled as basic elements, which then are connected by using straight and bent waveguides. Bent waveguides are important building blocks used to interconnect noncolinear straight waveguides and input/output ports, and they also are used in the designs of specialized components, such as ring resonators [1], arrayed waveguide filters [2], optical delay lines [3] and S-bend attenuators [4]. It is important to design a low-loss compact bend waveguide, such as an S-bend or a U-bend and to fold the guided wave sections to reduce the overall dimension of the PIC, which also reduces its fabrication cost. This procedure would also allow for a greater density of optical components onto the same overall "footprint" of the PIC, in order to increase its functionality and the reliability of the subsystems. Addressing these issues here, a rigorous study of various loss mechanisms in bent waveguides is presented.

Previous research [5] has shown that the field distribution of the fundamental mode in a bent waveguide is different from that of the straight waveguide. The radiation and transition losses between the straight and the bent waveguide contribute to the propagation properties of a bent waveguide. As a result, the power loss in a bent waveguide will be higher, due to the conversion of the incident beam to the higher order modes. By introducing an offset [6–8] for the input straight waveguide when coupled to a bent waveguide, the coupling or transition loss can be reduced. The unequal bending loss of the even and odd supermodes can also cause crosstalk in a directional coupler-based device [9]. Previously it has also been reported [10] that two polarized modes exchange power in bent waveguides causing polarization crosstalk. Bent waveguides are also deliberately used in the design of compact polarization rotators [11–14], which are important in the design of polarization-independent or polarization-diversity PICs, as they can be used to control the polarization state. Recent research has shown that hybrid optical modes exchange power between the polarization states if the modes are nearly phase-matched and have an enhanced overlap between them. However, to achieve power conversion, some forms of discontinuity such as bends, junctions, or tapers should exist along the propagation direction. Therefore, a polarization rotator may be made by using a number of uniform [15] or curved [16] butt-coupled waveguide sections to transfer power between the two polarized modes. This

0003-6935/08/162961-10$15.00/0

emphasizes the importance of a rigorous investigation of the polarization rotation in bent waveguides and thus is the basis of this work.

To undertake the analysis proposed, an accurate and efficient vector-**H**-field finite-element method (VFEM) [17] is first used to calculate the propagation constant and the full-vectorial modal field profiles of the straight and bent waveguides. Subsequently, the least squares boundary residual (LSBR) [18] method is employed to find the excited modal coefficients at the butt-coupled junction and finally the finite-element-based full-vectorial beam propagation method (FEBPM) [19] is used to find the polarization rotation and the power loss in the bent waveguides.

2. Theory

Curved optical waveguides have attracted increasing interest in the design of compact PICs, but the rigorous analysis of such bent waveguides is a challenging problem. Marcatili [20] has developed an approximate solution for the eigenvalue equation, by dividing the waveguide cross-section into several regions and using field expansion and field matching at the interfaces in order to obtain the curvature loss. Another simplified formula has been introduced by Marcuse [21] by utilizing a similar field expansion and field matching, but its validity is limited for a single-moded weakly guided waveguide with a sufficiently large bending radius.

Subsequently, to study arbitrary bends, various numerical methods have been developed and used to simulate the light propagation in bent waveguides with the aim of reducing the bending, transition, and polarization losses. The conformal transformation [22] has been used widely to represent bent waveguides by converting a curved dielectric waveguide to its equivalent straight waveguide with a modified index profile. Following that, a modal solution approach is necessary to find the modal solutions of the fundamental and higher order modes in both straight and bent waveguides and for this the eigenmode expansion [23], the method of lines [24,25], the finite difference method [26,27], the variational method [28], the matrix method [29], the Wentzel–Kramers–Brillouin analysis [30], and the beam propagation method (BPM) [31,32,8,7] have been used and also experimentally verified [31]. The finite-element method has also been employed using cylindrical coordinates with scalar [33] and vector **E**-field [34] formulations and the equivalent anisotropic refractive index approach [35]. Compact bends or rings can be modeled as resonators with rotational invariance [36,33], and using a cylindrical coordinate system [37], which is expected to be more accurate when the bending radius is comparable to the waveguide dimensions. Although the finite difference time-domain approach has also been used [38], these approaches are more computer intensive than the modal solution or BPM approach used herein.

For this particular semiconductor waveguide (with a strong index contrast), as shown in Fig. 1, the modal fields are hybrid in nature due to a significant non-dominant field component existing around the dielectric interfaces. Therefore a full-vectorial approach is necessary and has been used in this study to obtain modal solutions for straight and bent waveguides. The finite-element method based on the vector **H**-field formulation [17] has been established as one of the most accurate and numerically efficient approaches to obtain the modal field profiles and propagation constants of the fundamental and higher order quasi-TE and TM modes. The full-vectorial formulation is based on the minimization of the following functional [17] in terms of the nodal values of the full H-field vector:

$$\omega^2 = \frac{\int[(\nabla \times H)^* \cdot \varepsilon^{-1}(\nabla \times H) + p(\nabla \cdot H)^*(\nabla \cdot H)]\partial\Omega}{\int H^* \cdot \mu \mathrm{H} \partial\Omega}, \tag{1}$$

where **H** is the full-vectorial magnetic field, * denotes a complex conjugate and transpose, ω^2 is the eigenvalue, where ω is the angular frequency of the wave, and ε and μ are the permittivity and permeability, respectively. The penalty function approach has also been incorporated to impose a divergence-free condition of the magnetic field to reduce the appearance of spurious modes and p is the dimensionless penalty parameter. This full-vectorial FEM modal solution may also be used to determine the beat lengths between the fundamental and the higher order modes and also the polarization-beat length between the two quasi-TE and TM polarized fundamental modes.

The first step in the process is to transform the curved optical waveguide to an equivalent straight optical waveguide using the conformal transformation [22]. The coordinate transformation allows a bent optical waveguide in the x-plane to be represented by an equivalent straight waveguide with a modified refractive index distribution, $n'(x,y)$,

$$n'(x,y) = n_m(x,y)(1 - x/R), \tag{2}$$

where $n_m(x,y)$ is the original refractive index profile of the bent waveguide, $n'(x,y)$ is the equivalent index profile of a straight guide, R is the radius of the curvature, and x is the distance from the center of the waveguide.

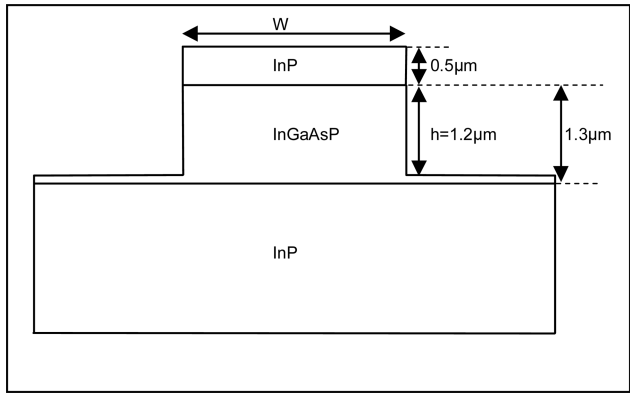

Fig. 1. Schematic cross-section of the bent optical waveguide.

At the junction between a straight and a bent waveguide besides the incident mode, other higher order modes can also be generated to satisfy the necessary boundary conditions. In this study a powerful numerical approach, the LSBR method [18] has been used, which rigorously satisfies the continuity of the tangential electric and magnetic fields at the junction interface and obtains the modal coefficients of the transmitted and reflected modes at the discontinuity interface. The LSBR method looks for a stationary solution to satisfy the continuity conditions by minimizing the error energy functional, **J**, as given by [18]

$$J = \int_{\Omega} |E_t^I - E_t^{II}|^2 + \alpha \cdot Z_0^2 |H_t^I - H_t^{II}|^2 \partial\Omega, \qquad (3)$$

where Z_0 is the free-space impedance and α is the dimensionless weighting factor to balance the electric and magnetic components of the error functional **J**. The integration is carried out at the junction interface, Ω, between the straight and the bent guides.

The beam propagation method (BPM) [19] is most widely used for the study of light propagation in optical waveguides, particularly through nonuniform and bent waveguides. Although a semivectorial BPM may yield polarization-dependent guiding properties, only a full-vectorial approach can identify the power coupling between the two polarization states. The finite-element-based full-vectorial BPM (FEBPM) [19] is used here to study the evolution of the optical beam in a bent waveguide for a given field excitation. From Maxwell's two curl equations, the vector wave equation based on the magnetic field vector **H** can be derived as [19]

$$\nabla \times (n^{-2} \nabla \times H) - k^2 H = 0, \qquad (4)$$

where ∇ is the del operator, and k and n are the free-space wave number and refractive index, respectively. In this work, after application of the conformal transformation, the 3 D curved waveguide is replaced by a simpler 3 D straight waveguide, butt-coupled to the input section.

To calculate the radiation loss in a bent waveguide, in this study a rigorous boundary condition incorporating the perfect matched layers (PML) [39] has been introduced around the orthodox computational window.

3. Results

The schematic cross section of a typical rib waveguide under investigation is shown in Fig. 1. This particular waveguide structure can be fabricated by growing a 1.3 μm thick InGaAsP guiding layer on top of the InP substrate. Additionally, a 0.5 μm InP cap layer can then be deposited on top of the InGaAsP guiding layer and subsequently a ridge can be etched with a core height of 1.2 μm. In the numerical simulations used, the width, W, is varied in order to understand its effect on modal field profiles and to study bending loss. The operating wavelength used in this analysis is 1.55 μm, and at this wavelength the refractive indices of the InGaAsP and the InP layers are taken as 3.27 and 3.17, respectively. All other parameter values of the waveguide are given in Fig. 1.

In this study, first the **H**-field based VFEM [17] is used to obtain the modal solutions of such waveguides. For this study, more than 20,000 first order triangular elements of different sizes have been used to represent the waveguide structure efficiently. For this waveguide, the fundamental quasi-TE ($H^y{}_{11}$) mode is more dominant than its equivalent quasi-TM ($H^x{}_{11}$) mode. The dominant H^y field component for $H^y{}_{11}$ (quasi-TE) mode is shown in Fig. 2(a) for the guide width $W = 3\,\mu$m. The field profile shows that the maximum intensity occurs at the center of the core. It is also shown that the field profile is symmetric along the vertical axis, where the field slightly extends towards the lower substrate region and also into the InP cap layer. The effective index, n_e, of the $H^y{}_{11}$ mode was found to be 3.23427. The effective index, n_e, of a given mode is a normalized propagation parameter, which can be defined as $n_e = \beta_0/k_0$, where β_0 is the propagation constant of a given mode and k_0 is the free-space wave number defined as $k_0 = \omega(\varepsilon_0\mu_0)^{1/2} = 2\pi/\lambda$. The spot size, σ, of this mode has been calculated to be 1.17 μm^2. Here the spot size, σ, is defined as the area where the power density is more than half of the maximum power density. The nondominant H^x field component of the quasi-TE ($H^y{}_{11}$) mode is shown in Fig. 2(b). As the H^x field is related to the spatial derivative of the dominant H^y field, it clearly shows four peak values with alternate positive and negative signs and at the center of the guide, an odd functional along the y-axis and a nearly odd functional in the x-direction. The maximum magnitude of the H^x field profile is very small and only 0.006 times the maximum value of the dominant H^y field.

Next, the VFEM is used to find the modal solution of a rib waveguide, bending towards the left side, as shown by the inset in Fig. 3(a). The dominant H^y field profile for the $H^y{}_{11}$ (quasi-TE) mode is shown in Fig. 3(a) for a bending radius, $R = 100\,\mu$m. In this case the modal field profile was obtained by using the VFEM after the conformal transformation [22] was applied to modify the equivalent index in the cross sectional plane of the rib waveguide. It clearly shows that the field in the core region shifts outward and is no longer symmetric, due to a higher equivalent index in the right and power leaks out at the lower-right side. The effective index of this mode (of the bent guide) is found to be 3.24346, which is higher than that of the straight waveguide. The spot size of this guide is found to be 0.8145 μm^2, which is smaller than that of the straight waveguide. The nondominant H^x field component for $H^y{}_{11}$ (quasi-TE) mode is shown in Fig. 3(b). It can be observed that the shape of the nondominant H^x field is similar to that of the dominant H^y field. The magnitude of this nondominant field in the bent guide is nearly 0.04 times that of the dominant field, which is also of a significantly higher magnitude compared to the same field in the straight waveguide. It also clearly shows that the field leaks towards the lower-right

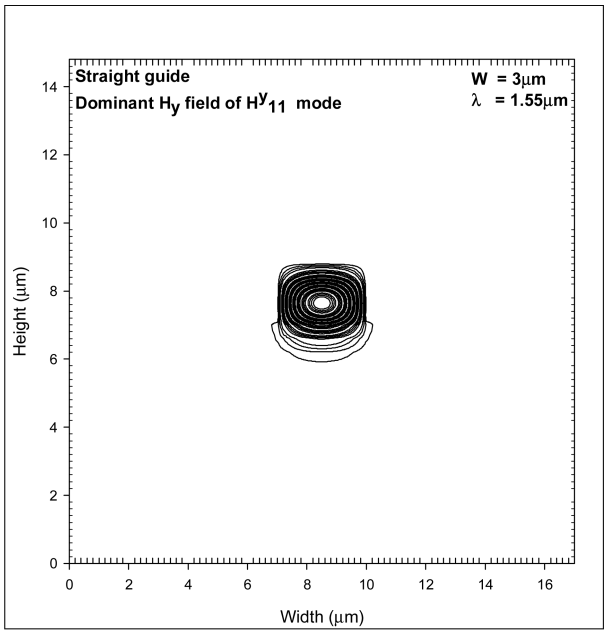

(a)

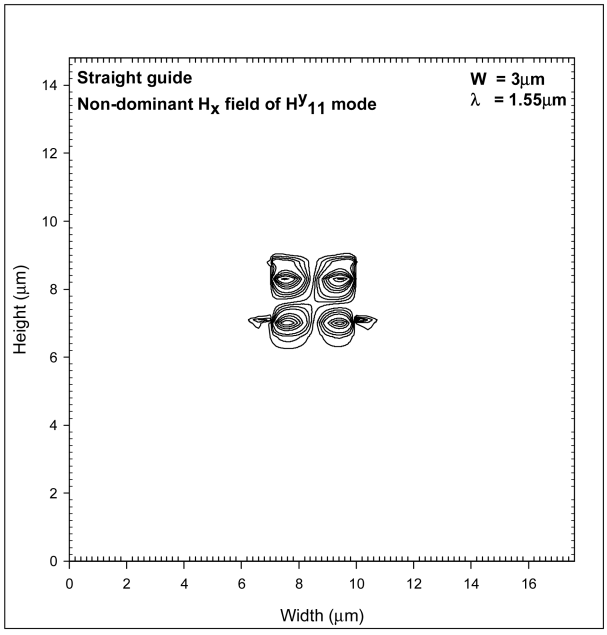

(b)

Fig. 2. (a) Dominant H_y field profile of the fundamental quasi-TE mode of a straight waveguide. (b) Nondominant H_x field profile of the fundamental quasi-TE mode of a straight waveguide.

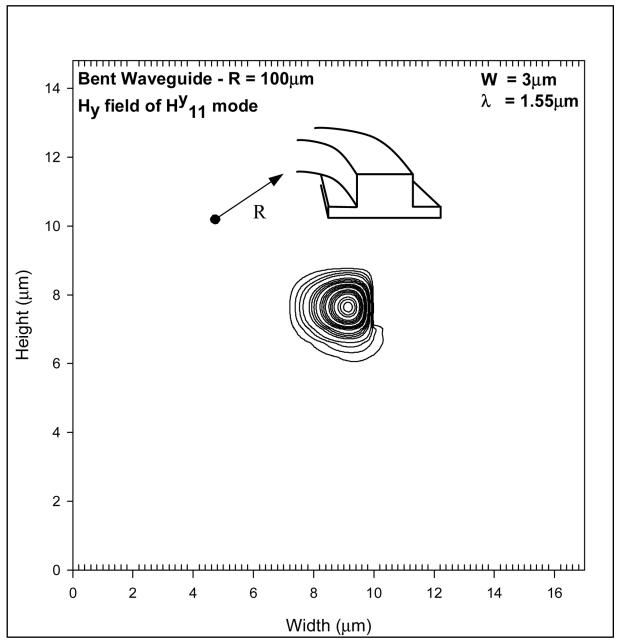

(a)

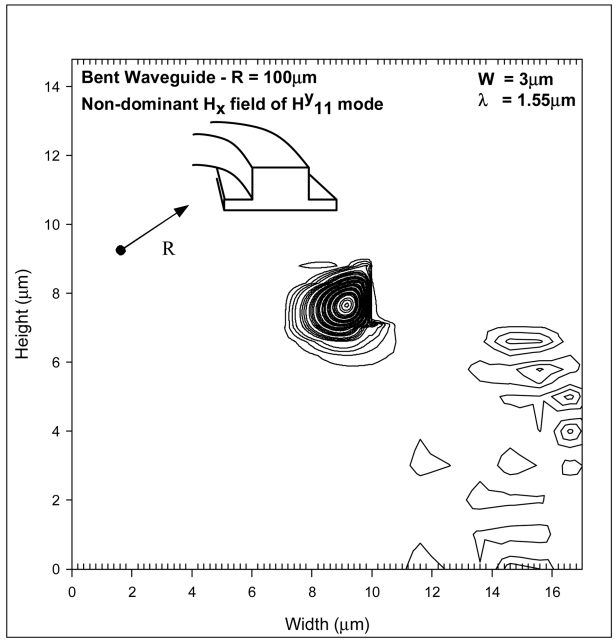

(b)

Fig. 3. (a) Dominant H_y field profile of the fundamental quasi-TE mode of a bent waveguide. (b) Nondominant H_x field profile of the fundamental quasi-TE mode of a bent waveguide.

corner. Similarly, for the quasi-TM $H^x{}_{11}$ mode, both the dominant H^x and the nondominant H^y field profiles are of similar shapes but these are not shown here. Since the dominant and nondominant field profiles are similar in shape and the magnitude of the nondominant component is higher in a bent waveguide, the overlap integral between the vector modal fields of the $H^y{}_{11}$ and $H^x{}_{11}$ modes is expected to be higher and, as a result, the power conversion between these two polarized modes will increase.

Next, to find the leakage loss of a bent rib waveguide, the FEBPM [19] is used. In this study, the fundamental $H^y{}_{11}$ modal field profile of the straight guide, obtained by using the VFEM [17] is used as the input field to launch into the FEBPM code [19], where the conformal transformation has also been used to represent a bent waveguide. The variation of the power loss for a straight-to-bent waveguide along the propagation distance is shown in Fig. 4. Initially, the rate of the power loss is about

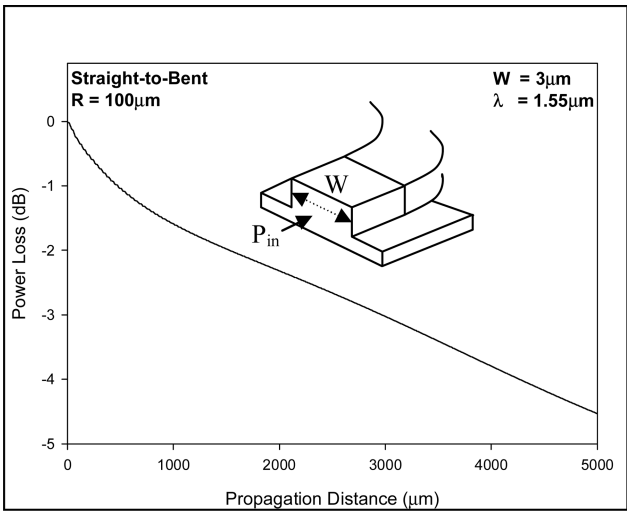

Fig. 4. Variation of the power loss along the axial distance for a straight-to-bent waveguide.

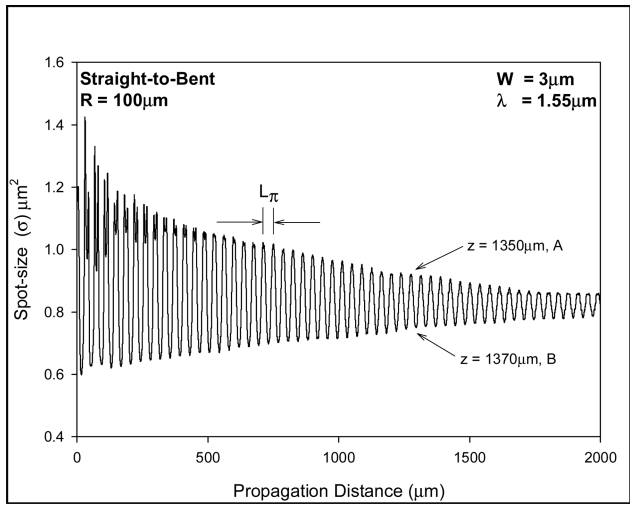

Fig. 5. Variation of the spot size along the axial distance for a straight-to-bent waveguide.

2.2 dB/mm when the guide contains both the fundamental and the higher order modes. As the field propagates further down the bent waveguide, the rate of power loss is clearly seen to be reduced as the optical beam strips off the more lossy higher order modes and it mostly contains the fundamental mode in this location. It can be observed that the average loss value is about 0.74 dB/mm between the axial distances of 4000 to 5000 μm.

The variation of the spot size along the propagation distance is shown in Fig. 5 when a mode from the straight guide is launched into the bent guide. Rapid oscillations of the spot size can be observed in the first 1000 μm and as the propagation distance increases, the spot size appears to show damped oscillations and settles at around 0.82 μm^2, where this value is also very similar to the value obtained by using the VFEM for a bent waveguide. The output field profile is not shown here but at $z = 2000\,\mu$m; it was observed to be similar to the modal field profile of the bent guide, which was shown in Fig. 3(a). The periodic change of the spot size has a beat length of 20 μm. This period clearly correlates with $L_\pi = \pi/\Delta\beta = 19\,\mu$m, where $\Delta\beta$ is the difference between the propagation constants of the $H^y{}_{11}$ and $H^y{}_{21}$ modes calculated by using the VFEM. This clearly demonstrates that at the junction of a straight-to-bent waveguide, the higher order $H^y{}_{21}$ mode is generated. The oscillations in the spot size have occurred because of the mode beating between the fundamental mode and the higher order modes.

To quantify the magnitudes of the higher order modes generated, the LSBR method [18] is employed next. Since the dominant mode in the bent guide is different from the input field of the straight guide, the higher order modes are excited to satisfy the necessary boundary conditions. The modal coefficients of the $H^y{}_{11}$ and $H^y{}_{21}$ modes obtained using the LSBR method are 0.89 and 0.38, respectively. This shows that although the fundamental $H^y{}_{11}$ mode is dominant, the other modes also are excited and propagate along with the fundamental mode. When the propagation distance is more than 500 μm, the optical field mostly contains the $H^y{}_{11}$ mode with a significantly attenuated $H^y{}_{21}$ mode. On the other hand, a small amount of the $H^y{}_{31}$ mode is also excited, but being very close to its modal cutoff it leaks out very quickly, which correlates with the secondary peaks that exist at an early stage, between a propagation distance of 0 and 400 μm. To validate further the mode beating, the difference between the field profiles at axial positions A (at $z = 1350\,\mu$m) and B (at $z = 1370\,\mu$m), as identified in Fig. 5, where the $H^y{}_{21}$ mode has gone through phase reversal, is shown in Fig. 6, which clearly shows that this field profile is similar to that of the $H^y{}_{21}$

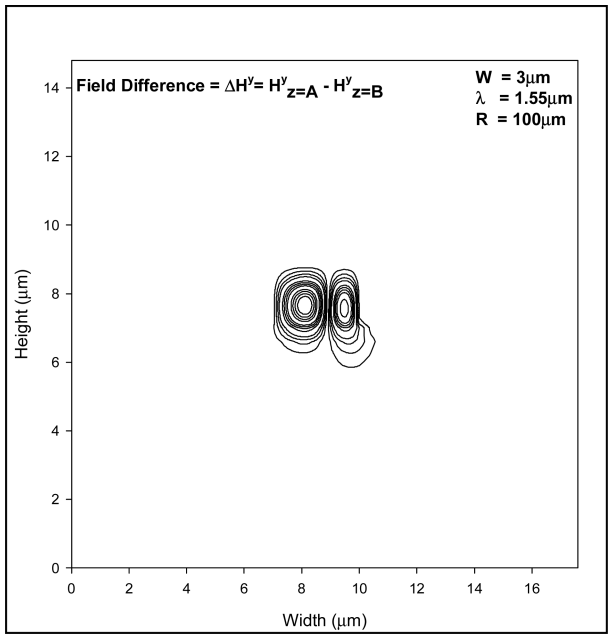

Fig. 6. Difference between two H_y field profiles at two locations with a phase reversal.

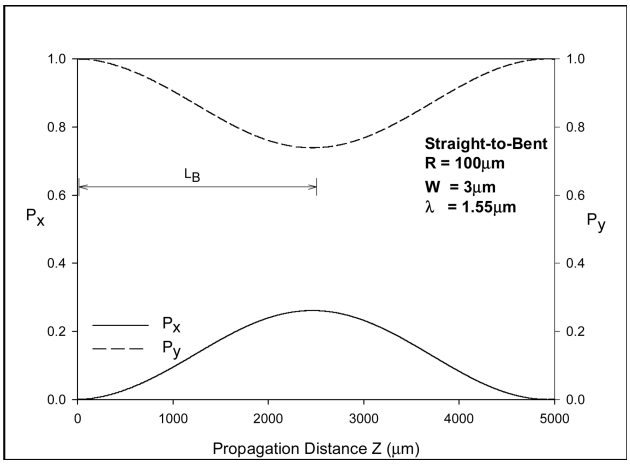

Fig. 7. Evolutions of the y and x-polarized powers along the axial distance.

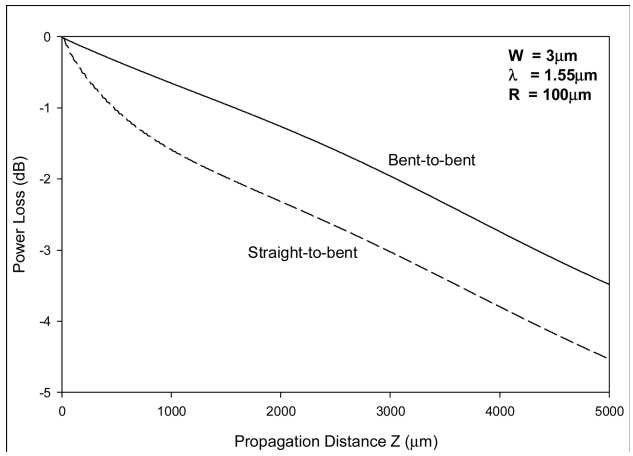

Fig. 8. Variations of power losses along the axial distance for bent-to-bent and straight-to-bent waveguides.

mode in a bent guide mode and that it leaks out into the lower right-hand corner.

A bent waveguide is also known to exchange power between the two polarization states [10]. A FEBPM [19] with perfectly matched layer boundary conditions has been used here to find the TE-to-TM power conversion. The evolution of the quasi-TE and TM powers along the axial direction is shown in Fig. 7 for straight-to-bent waveguide coupling. In this case, since the quasi-TE ($H^y{}_{11}$) mode was incident at the start of the bent waveguide ($z = 0$), the H^x-polarized normalized power, P_x, is nearly zero and the H^y-polarized normalized power, P_y, is nearly one. As the modes propagate along the bent waveguide section, this shows that the maximum polarization conversion occurs at $z = 2500\,\mu$m, which correlates well with the polarization-beat length $L_B = \pi/|\beta_y - \beta_x|$, obtained by using the VFEM, where β_y and β_x are the propagation constants of the fundamental $H^y{}_{11}$ and $H^x{}_{11}$ modes in the bent waveguide, respectively.

Next, to quantify the bending loss only, the butt coupling between an imaginary bent-to-bent waveguide is studied. In this case, the mode profile of the bent waveguide is obtained by using the VFEM [17] (after a conformal transformation of the input guide) and this profile is launched into the BPM code [19] representing the bent guide (also using the conformal transformation). The variation of the power loss along the propagation distance is shown in Fig. 8 by a solid line. In this case, the power loss is less than that of the straight-to-bent waveguide coupling, since the loss in a straight-to-bent also includes the loss due to the field mismatch. For comparison, the loss for the straight-to-bent guide, as shown earlier in Fig. 4, is also shown here by a dashed line. It can be observed that for $z > 2$ mm, the slopes of both the curves are similar, because in the straight-to-bent case, the magnitudes of the higher order modes that remained beyond this position are very small and, therefore, the loss rates near the end are similar. As can be seen from the bent-to-bent graph, the rate of power loss of the pure $H^y{}_{11}$ mode (of a bent guide) is nearly uniform, with a value of 0.68 dB/mm.

To quantify the overall loss, the loss value for the $H^y{}_{21}$ mode was also obtained by launching this mode profile into the FEBPM code and found to be 10.61 dB/mm. For a straight-to-bent coupling, at the start in the bent section the transmitted field contained 79% of the power in the $H^y{}_{11}$ mode, 14% of the power in the $H^y{}_{21}$ mode, and the rest in the higher order radiating modes. With the modal loss values calculated as 0.68 dB/mm and 10.61 dB/mm for the $H^y{}_{11}$ and $H^y{}_{21}$ modes, respectively, in the bent waveguide, and their power fractions being 85% and 15%, respectively, this gives an overall loss value of 2.17 dB/mm, which agrees very well with the loss value of 2.2 dB/mm, as shown in Fig. 4 at $z = 0$. In both cases, the fundamental $H^y{}_{11}$ mode suffers the same bending loss; however, for the straight-to-bent case, which contains nearly 21% of the power in the higher order guided and radiated modes, this part of the power is quickly lost, which is clearly shown in Fig. 8 as the additional 1.05 dB loss near the end, at $z = 5$ mm.

For the bent-to-bent coupling, the spot size along the propagation distance was constant, but this is not shown here. However, the constant value of $0.824\,\mu\text{m}^2$ agrees well with the spot size value of $0.82\,\mu\text{m}^2$ calculated by using the VFEM for a bent guide. In this case, since no higher order mode was excited, there was no mode beating and such a process was responsible for the periodic variation of the spot size, as shown in Fig. 5.

Power loss critically depends on the bending radius and the way the input and the output sections are coupled. The variations of the total power loss values for a straight-to-bent and a bent-to-bent coupler with a 1 mm bent section are shown in Fig. 9. The total loss value for the straight-to-bent coupling is shown by a dashed curve. On the other hand, for the bent-to-bent waveguide coupling, the loss values are shown by a solid curve. It is shown here that, in both cases, as the radius, R, decreases, the loss

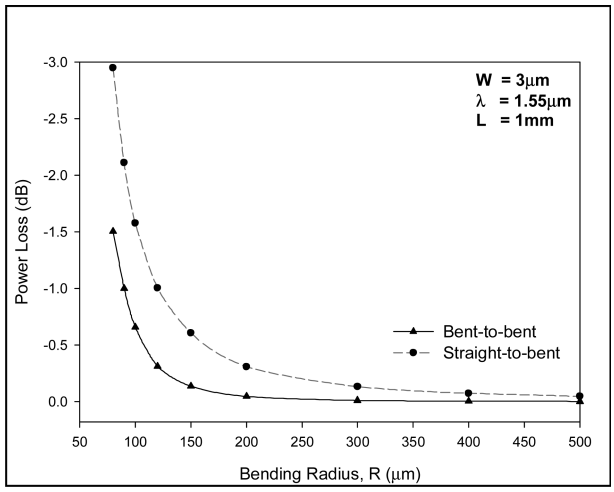

Fig. 9. Variation of the power losses with the bending radius for straight-to-bent and bent-to-bent waveguides.

values increase and it can also be seen that the loss is higher for a straight-to-bent coupling. In this case the additional loss is due to the field mismatch at the discontinuity junction, as mentioned earlier. It has also been noted that the difference between the two sets also increases with the reduction of the bending radius as the more modified field profile in the bent guide increases the field mismatch loss.

It was also shown in Fig. 7 that such a bent waveguide suffers from the periodic exchange of power between the polarized modes. Often this can increase the polarization crosstalk in an optoelectronic system comprising bent sections. On the other hand, such bent waveguides can be deliberately used to rotate the polarization state of an incoming signal. The variation of the maximum polarization conversion with the bending radius is shown in Fig. 10. It can be clearly observed that as the bending radius decreases, the polarization conversion increases. However, the polarization conversions are similar for both cases, whether the input waveguide is straight or bent. This suggests that the polarization conversion primarily depends on the bending radius. To keep the polarization crosstalk below an acceptable level, the maximum allowable bending radius has to be designed carefully. In this case, the bending radius should be larger than 270 μm to keep the polarization crosstalk better that—20 dB. However, for the design of a polarization rotator, the objective is to maximize the polarization conversion with minimum power loss. It may, however, be difficult to achieve 100% polarization conversion using a single section polarization rotator design by reducing the bending radius appreciably, as in this case the power loss would also increase significantly. In such a case, several bent sections can be cascaded [16] with phase reversal at a regular interval equal to the polarization-beat length, L_B. However, most of the earlier work has only mentioned the normalized power conversion between the polarized modes (ignoring the power loss); our present study shows a significant power loss for compact bent sections, which, it should be stressed, cannot be ignored.

In the discussion above, it is shown that radiation loss primarily depends on the bending radius and the additional loss arises due to the mismatch between the fields on the both sides of a junction. Since it would not be possible in a practical case to excite the bent section by launching a field similar to that of the bent waveguide, several approaches have been reported to reduce such losses. One of these approaches is created by introducing a lateral offset between the straight and bent guides [6–8]. In this case, an offset is introduced where the input straight waveguide is shifted to the right when coupling to the bent waveguide to enhance the field matching (since the modal field of a bent guide shifts outward). The inset diagram in Fig. 11 shows how this offset can be achieved. It can be observed that, as the offset, Δx, increases, the total loss initially reduces and reaches its minimum value before the loss starts increasing. It can be observed that the minimum loss is achieved when the offset $\Delta x = 0.19\,\mu$m, where the

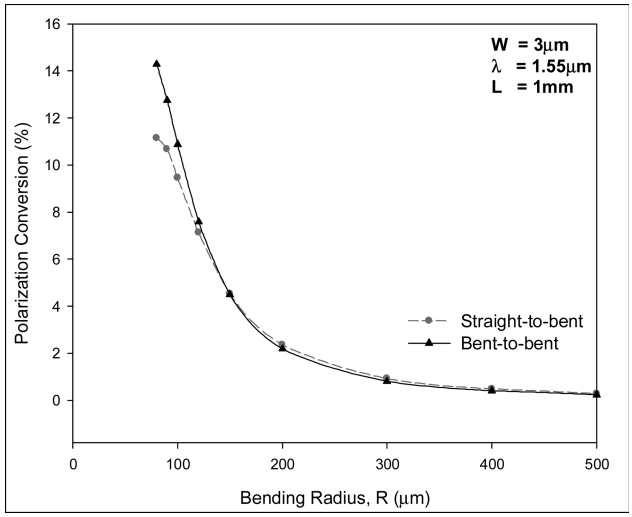

Fig. 10. Variation of the polarization conversions with the bending radius.

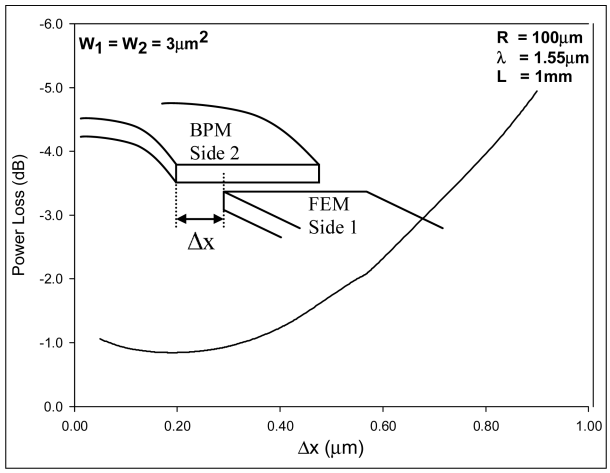

Fig. 11. Variation of the power loss for a straight-to-bent coupled waveguide with the waveguide offset, Δx.

field matching is at an optimum and the minimum loss value is 0.84 dB. As mentioned earlier, this loss contains the bending loss of the fundamental mode and the higher order modes and also the loss due to field mismatch between two coupling waveguides. Using the LSBR method [18], the modal coefficients of the $H^y{}_{11}$ and $H^y{}_{21}$ modes were calculated to be 0.923 and 0.2706, respectively, when $\Delta x = 0.19\,\mu$m. Therefore for this design optimization, the bent guide will contain about 85% of the power in the $H^y{}_{11}$ and only 7.3% power in the $H^y{}_{21}$ modes with the remaining power existing in higher order radiation modes. It has also been observed that polarization conversion reduces significantly when the waveguide offset is introduced.

It was shown in Fig. 3(b) that the mode shape in a bent guide not only shifts outward, but also shrinks, and, next, an alternative offset method is studied, where the width of the input waveguide is reduced to improve the mode matching. The inset diagram in Fig. 12 demonstrates how this particular offset was achieved. It can be observed that as the width of the input waveguide decreases from 3 μm, the width difference, Δw, increases and the loss value decreases until it reaches its minimum, following which the loss value again increases. The optimum offset, Δw, in this case is found to be 0.73 μm when the minimum loss value of 0.619 dB is attained. It should be noted that most of the earlier work [6–8] reports only on the reduction of the transition loss by introducing an offset between the straight and curved section, but this study shows, for what is believed to be the first time, that by using waveguides of unequal width, the transition loss can also be reduced significantly.

The variation of the spot size for the straight-to-bent waveguide, but with $\Delta w = 0.73\,\mu$m, is shown in Fig. 13. For this case, the coefficient for the $H^y{}_{11}$ is increased to 0.977 and that of the $H^y{}_{21}$ mode is reduced to only 0.10, calculated by using the LSBR method. It should be noted that in this case the power carried by the $H^y{}_{21}$ mode is only 1% as compared to a significantly larger value of 14% when

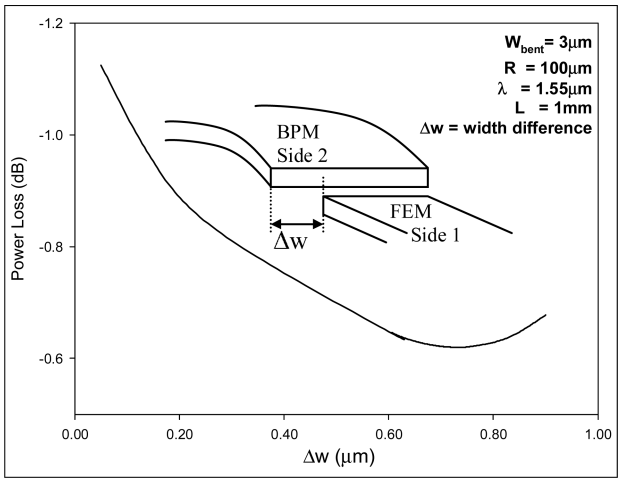

Fig. 12. Variation of the power loss for a straight-to-bent waveguide with Δw when the waveguide widths are unequal.

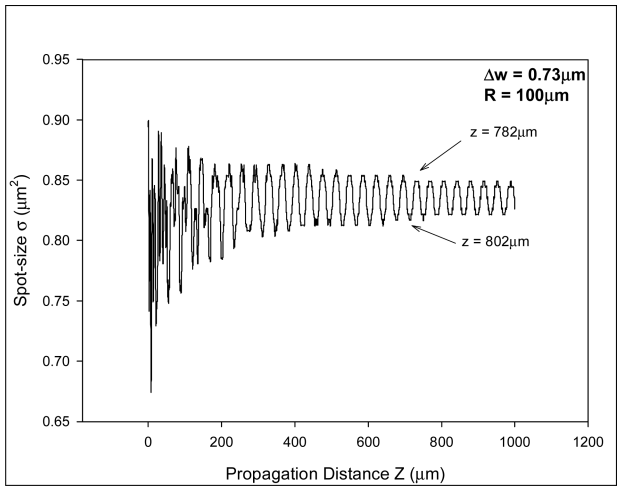

Fig. 13. Variation of the spot size along the axial direction when an optimized value of Δw is used.

$\Delta w = 0$. Figure 13 clearly shows the spot size varies around $\pm 1.7\%$, compared to more than $\pm 12.6\%$ for $\Delta w = 0$, which was shown in Fig. 5. For many devices, the periodic pulsation of the spot size also varies the local power density and this can bring detrimental nonlinear effects such as gain saturation or facet damage. It has also been observed that polarization conversion is only 0.4% when the optimized unequal waveguide width is used.

For a specific design optimization, both the width change and offset can be incorporated simultaneously to reduce the bending loss, the transition loss, and also the mode beating. Similarly, side trench [40] or index contouring using multilayers with a different refractive index profile [41] can be used to increase the modal confinement in the outward side (here on the right side) to reduce the bending loss.

4. Conclusion

The rigorous full-vectorial modal solution, junction analysis, and BPM approaches have been used to study the bending loss, the transition loss, and the polarization conversion in a bent high index contrast semiconductor optical waveguide. It has been shown that a reduction in the bending radius increases the modal loss and the associated transition loss also increases as the mode shape modifies significantly in the bent waveguide. Rigorous full-vectorial characterization and design optimization of compact bent waveguides, to allow the highest degree of integration yet keep the excess bending loss, transition loss, optical crosstalk, and polarization crosstalk within an acceptable limit, are possible. It is also shown here that the transition losses and polarization conversion can be reduced by using both a narrower input guide and an appropriate offset. For a specific PIC structure, both the narrow input waveguide and the appropriate offset can be introduced simultaneously, and the numerical approaches presented here are suitable to carry out such an optimization using the computationally efficient finite-element-based approaches.

In a bent waveguide, the nondominant field component is relatively large compared to that in a straight waveguide; its shape is also similar to that of the dominant field, so the overall integral between the two vector modal fields of the quasi-TE and TM modes is significantly higher. It is also shown that when the bending radius is reduced to design a compact PIC, the associated polarization conversion also increases significantly. However, by reducing the bending radius, a polarization rotator can be designed, but it is also shown here that such devices suffer from a significant amount of power loss in the bent section. On the other hand, by incorporating single or several cascaded bent sections with vertical or slanted side walls and with an optimized offset design or width difference, a compact and low-loss polarization rotator can be designed effectively.

References

1. B. E. Little, S. T. Chu, H. A. Haus, J. Foresi, and J. P. Laine, "Microring resonator channel dropping filters," J. Lightwave Technol. **15**, 998–1005 (1997).
2. M. Zirngibl, C. H. Joyner, L. W. Stulz, Th. Gaiffe, and C. Dragone, "Polarization independent 8 × 8 waveguide grating multiplexers on InP," Electron. Lett. **29**, 201–202 (1993).
3. R. R. Hayes and D. Yap, "GaAs spiral optical waveguides for delay-line applications," J. Lightwave Technol. **11**, 523–528 (1993).
4. X. Jiang, W. Qi, H. Zhang, Y. Tang, Y. Hao, J. Yang, and M. Wang, "Loss crosstalk 1 × 2 thermooptic digital optical switch with integrated S-bend attenuator," IEEE Photon. Technol. Lett. **18**, 610–612 (2006).
5. W. A. Gambling, H. Matsumura, and C. M. Ragdale, "Field deformation in a curved single-mode fibre," Electron. Lett. **14**, 130–132 (1978).
6. E. C. M. Pennings, G. H. Manhoudt, and M. K. Smit, "Low-loss bends in planar optical ridge waveguides," Electron. Lett. **24**, 998–999 (1988).
7. V. Subramaniam, G. N. De Brabander, D. H. Naghski, and J. T. Boyd, "Measurement of mode field profiles and bending and transition losses in curved optical channel waveguides," J. Lightwave Technol. **15**, 990–997 (1997).
8. M. Rajarajan, S. S. A. Obayya, B. M. A. Rahman, K. T. V. Grattan, and H. A. El-Mikathi, "Characterization of low-loss waveguide bends with offset optimisation for compact photonic integrated circuits," IEE Proc.-Optoelectron. **147**, 382–388 (2000).
9. J. C. Powelson, W. Feng, S. Lin, R. J. Feuerstein, and D. Tomic, "Crosstalk of passive directional couplers," J. Lightwave Technol. **16**, 2020–2027 (1998).
10. C. Yeung, T. Rozzi, and G. Cerri, "Crosspolarisation coupling in curved dielectric rib waveguides," IEE Proc.-Optoelectron. **135**, 281–284 (1988).
11. C. van Dam, L. H. Spiekman, F. P. G. M. van Ham, F. H. Groen, J. J. G. M. van der Tol, I. Moerman, W. W. Pascher, M. Hamacher, H. Heidrich, C. M. Weinert, and M. K. Smit, "Novel compact polarization converters based on ultra short bends," IEEE Photon. Technol. Lett. **8**, 1346–1348 (1996).
12. W. W. Lui, T. Hirono, K. Yokoyama, and W. P. Huang, "Polarization rotation in semiconductor bending waveguides: a coupled-mode theory formulation," J. Lightwave Technol. **16**, 929–936 (1998).
13. B. E. Little and S. T. Chu, "Theory of polarization rotation and conversion in vertically coupled microresonators," IEEE Photon. Technol. Lett. **12**, 401–403 (2000).
14. S. S. A. Obayya, B. M. A. Rahman, K. T. V. Grattan, and H. A. El-Mikati, "Improved design of a polarization converter based on semiconductor optical waveguide bends," Appl. Opt. **40**, 5395–5401 (2001).
15. N. Somasiri, B. M. A. Rahman, and S. S. A. Obayya, "Fabrication tolerance study of a compact passive polarization rotator," J. Lightwave Technol. **20**, 751–757 (2002).
16. S. S. A. Obayya, B. M. A. Rahman, K. T. V. Grattan, and H. A. El-Mikathi, "Analysis of polarisation rotation in cascaded optical waveguide bends," IEE Proc.-Optoelectron. **149**, 75–80 (2002).
17. B. M. A. Rahman and J. B. Davies, "Finite element solution of integrated optical waveguides," J. Lightwave Technol. **2**, 682–688 (1984).
18. B. M. A. Rahman and J. B. Davies, "Analysis of optical waveguide discontinuities," J. Lightwave Technol. **6**, 52–57 (1988).
19. S. S. A. Obayya, B. M. A. Rahman, K. T. V. Grattan, and H. A. El-Mikati, "New full-vectorial numerically efficient propagation algorithm based on the finite element method," J. Lightwave Technol. **18**, 409–415 (2000).
20. E. A. J. Marcatili, "Bends in optical dielectric guides," Bell Syst. Tech. J. **48**, 2103–2132 (1969).
21. D. Marcuse, "Curvature loss formula for optical fibers," J. Opt. Soc. Am. **66**, 216–220, (1976).
22. M. Heiblum and J. H. Harris, "Analysis of curved optical waveguides by conformal transformation," IEEE J. Quantum Electron. **11**, 75–83 (1975).
23. P. Bienstman, E. Six, M. Roelens, M. Vanwolleghem, and R Baets, "Calculation of bending losses in dielectric waveguides using eigenmode expansion and perfectly matched layers," IEEE Photon. Technol. Lett. **14**, 164–166 (2002).
24. J. Gu, P. Besse, and H. Melchior, "Novel method for analysis of curved optical rib-waveguides," Electron. Lett. **25**, 278–280 (1989).
25. R. Pregla, "The method of lines for analysis of dielectric waveguide bends," J. Lightwave Technol. **14**, 634–639 (1996).
26. S. Kim and A. Gopinath, "Vector analysis of optical dielectric waveguide bends using finite-difference method," J. Lightwave Technol. **14**, 2085–2092 (1996).
27. A. Nesterov and U. Troppenz, "A plane-wave boundary method for analysis of bent optical waveguides," J. Lightwave Technol. **21**, 2434–2437 (2003).
28. F. Wassmann, "Modal field analysis of circularly bent single-mode fibers," J. Lightwave Technol. **17**, 957–968 (1999).
29. K. Thyagarajan, M. R. Shenoy, and A. K. Ghatak, "Accurate numerical method for the calculation of bending loss in optical waveguides using a matrix approach," Opt. Lett. **12**, 296–298 (1987).
30. W. Berglund and A. Gopinath, "WKB analysis of bend losses in optical waveguides," J. Lightwave Technol. **18**, 1161–1166 (2000).
31. R. T. Schermer and J. H. Cole, "Improved bend loss formula verified for optical fiber by simulation and experiment," IEEE J. Quantum Electron. **43**, 899–909 (2007).
32. R. Baets and P. E. Lagasse, "Loss calculation and design of arbitrarily curved integrated-optic waveguides," J. Opt. Soc. Am. **73**, 177–182 (1983).
33. T. Yamamoto and M. Koshiba, "Numerical analysis of curvature loss in optical waveguides by the finite-element method," J. Lightwave Technol. **11**, 1579–1583 (1993).
34. R. Jedidi and R. Pierre, "High-order finite-element method for the computation of bending loss in optical waveguides," J. Lightwave Technol. **25**, 2618–2630 (2007).
35. Y. Tsuji and M. Koshiba, "Complex modal analysis of curved optical waveguides using a full-vectorial finite element method with perfectly matched layer boundary conditions," Electromagnetics **24**, 39–48 (2004).

36. L. Prkna, M. Hubalek, and J. Ctyroky, "Field modelling of circular microresonators by film mode matching," IEEE J. Sel. Top. Quantum Electron. **11**, 217–223 (2005).
37. K. Kakihara, N. Kono, K. Saitoh, and M. Koshiba, "Full-vectorial finite element method in cylindrical coordinate system for loss analysis of photonic wire bends," Opt. Express **14**, 11128–11141 (2006).
38. N. H. Vu, I-K. Hwang, and Y-H. Lee, "Bending loss analyses of photonic crystal fibers based on the finite-difference time-domain method," Opt. Lett. **33**, 119–121 (2008).
39. J. P. Berenger, "A perfectly matched layer for the absorption of electromagnetic waves," J. Comput. Phys. **114**, 185–200 (1994).
40. M. Rajarajan, S. S. A. Obayya, B. M. A. Rahman, K. T. V. Grattan, and H. A. El-Mikathi, "Design of compact optical bends with a trench by use of finite element and beam propagation methods," Appl. Opt. **39**, 4946–4953 (2000).
41. S. Tomlijenovic-Hanic, J. D. Love, and A. Ankiewicz, "Effect of additional layers on bend loss in buried channel waveguides," IEE Proc.-Optoelectron. **150**, 259–265 (2003).